



Phytofiltration of Rhodamine-B dye using microwave-assisted tartaric acid-treated *Trapa natans* peels from waste water by biosorption

Asfa Bajwa¹ · Rabia Rehman¹ · Sibgha Ayub¹ · Muhammad Raza Malik¹ · Sabah Ansar² · Liviu Mitu² · Fadi Alakhras^{3,4}

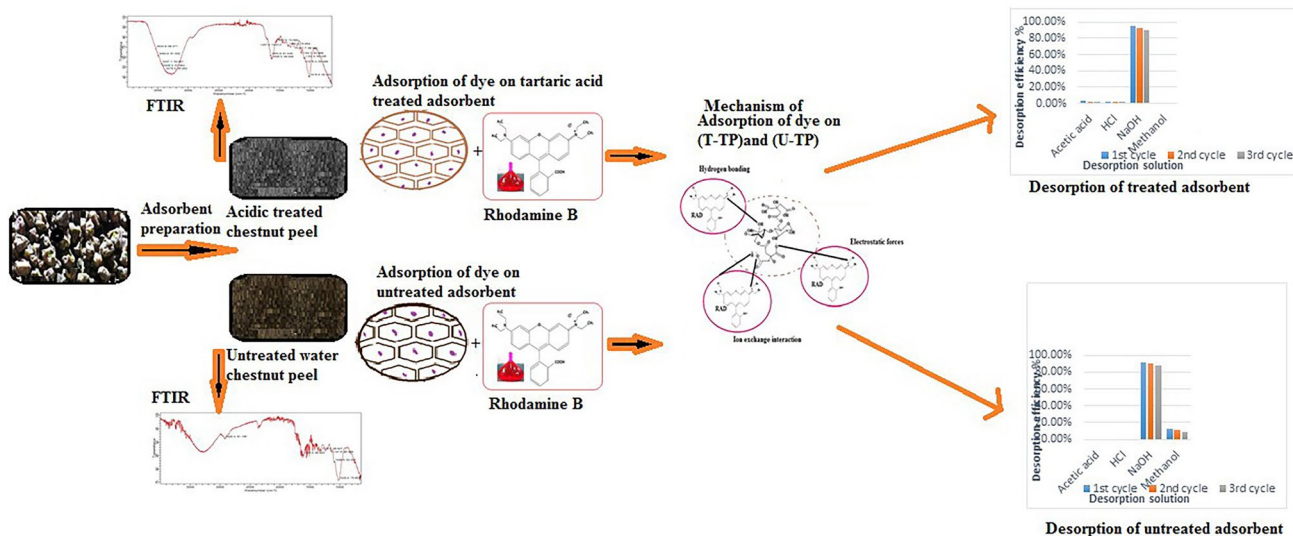
Received: 21 June 2024 / Accepted: 4 September 2024

© The Author(s), under exclusive licence to Springer-Verlag GmbH Germany, part of Springer Nature 2024

Abstract

Global pollution of water has increased as a result of fast industrial and population expansion, especially in the textile sector where artificial dye use and coloring ingredient discharge have increased significantly. The following research presents the adsorption effectiveness of the adsorbent in the elimination of Rhodamine-B from aqueous solutions and industrial effluent. Adsorbents were water chestnut peel powders in the form of simple and modified peels. Using plain peels at pH 1 and tartaric acid-modified chestnut peels at pH 3, batch adsorptive removal of the dye was optimized. It was discovered that the ideal adsorbent dose for simple and treated peels, respectively, was 1.4 g and 2.0 g. The sorbent efficiency for Rhodamine-B dye was investigated by optimizing several parameters, including agitation speed, pH, temperature, and sorbent dosage. In batch mode processing, simple and acid-modified biosorbent was used to get rid of dangerous basic dye, like: Rhodamine-B. The Langmuir model turned out to have the best fit to equilibrium experimental data when compared to isothermal computational models, which had Q_{max} values of 2.8801 and 5.5803 mg/g for Rhodamine-B with simple and treated peels, respectively. Since homogenous and monolayer adsorption results between the adsorbate molecules and the adsorbent surfaces through chelation and interaction of ion mechanisms, the process ideally follows pseudo-2nd-order kinetics. For the adsorption performance of both biosorbents (simple and treated peels), thermodynamic parameters are calculated statistically. These data indicate that the biosorption processes are both endothermic and spontaneous.

Graphical abstract



Keywords *Trapa natans* · Rhodamine-B dye · Dye removal

Extended author information available on the last page of the article

Published online: 11 September 2024

Abbreviations

TP	<i>Trapa natans</i> peels
U-TP	Untreated <i>Trapa natans</i> peels
T-TP	Tartaric acid-treated <i>Trapa natans</i> peels
RAD	Rhodamine-B dye
MRFR	Market Research Future Reports

Introduction

The global textile industry is well-known for bringing in over US\$1000 billion annually (Zhang et al. 2023), and the market for textile goods is estimated to account for around 2% of the world's gross domestic product. Since the textile industry is the second most polluting industrial sector in today's civilization, the majority of hazardous and permanent environmental issues arise. Similarly, using industrial dyes excessively—dyes used in dyeing—affects human health; these dyes are then flushed away as wastewater. Textile colors contribute between 10 and 45% of the discharge effluent.

All over the world, textile industrial units use more than 10,000 tons of dyes a year; yet, following the dyeing process, their wastewater is estimated to include 1000 tons of dye effluents every year, which significantly contaminates water resources (Mansour et al. 2021). The industries that release the most dye effluents into the environment these days are tanning and paint (8%), paper and pulp (9%), dyeing (21%), and the textile sector (55%), with the dye production industries accounting for 7% of this total. Most dyes are discharged from the textile sector. The comprehensive analysis conducted by MRFR indicates that the global textile colorants market is projected to expand at a compound annual growth rate of 8.13 between 2016 and 2023.

One of the most widely used and reasonably priced textile industry dyes for printmaking, making textiles, and as a coloring agent is Rhodamine-B (Lellis et al. 2019). It illustrates the way to use mark inks, ballpoint pens, leather, paper coloring, and stone dyeing (Imam and Babamale 2020). Because Rhodamine-B solution is not biodegradable, it is referred to as a persistent organic pollutant (Yang et al. 2021). Previous studies have shown that drinking water contaminated with dye effluents, such as: Rhodamine-B (RAD) can cause skin rashes, acute poisoning, digestive issues, failure of the liver, and dyspnea (Senol et al. 2023). In addition, these chemicals pose a serious risk to human health and are exceedingly cancer-causing and poisonous. It is important to note that organic dyes in the environment have an impact on plant metabolism and physiological functions, which can lead to an imbalance in loads and plant inhibition (Sharma et al. 2022). The environmental risks associated with the untreated disposal of azo dyes stem from their metabolites, aromatic amines, which are highly carcinogenic and have a

substantial impact on human health. Thus, in order to protect the lives of adults and newborns, it is necessary that toxic, dangerous, deadly, fatal, and irreversible effluents are removed from water streams as soon as possible.

There are two kinds of dyes on the market: synthetic and natural. At the dawn of civilizations, colors came from natural sources, such as: plants like: madder (*Rubia tinctorum*) (Ozdemir and Karadag 2023), beetroot red (*Betanin*) (Cabas and Icier 2021), Hina (*Lawsonia inermis* L.) (Kolahalam et al. 2024), safflower (*Carthamus tinctorius*) (Pannacci et al. 2024), activated almond shell (SAS) and raw almond shells (*Prunus amygdalus*) (Coskun et al. 2018) saffron (*Crocus sativus*) (Askary et al. 2024), yellow mustard seed (*Sinapis alba*) (Savci, 2017), pulp (*Nigella sativa*) (Seçme and Savci, 2018), logwood (Hasanah and Islam 2024), fish bone (*Sparus aurata*) (Savci and Kemiklioglu 2017), pomegranate rind (*Punica granatum*) (Gupta 2019), or animal sources, like: insects (*Kerriidae*), cochineal (*Dactylopius coccus*), sea snails, Kermes, and shellfish (AlAshkar and Hassabo 2021). As a consequence of the development of an information-driven, modern society, the synthesized substances causing the color were discovered.

The molecular functional groups in the visible spectrum that capture light, which is 400–800 nm in wavelength, that give rise to color, may now be identified by researchers. Based on their structural characteristics, synthetic dyes can be designated anthraquinone, azo, dispersion, acidic, basic, or direct dyes. Anionic, cationic, and non-ionic dyes are further classifications for these structural variations in dyes (Affat 2021). The cationic basic dye Rhodamine-B (RAD) is a commonly used member of the anthraquinone class (Wang and Gu 2018). In order to eliminate dyestuffs from water, a variety of physical and chemical techniques have been used, including electrochemical oxidation, precipitation, ozonolysis, coagulation-flocculation, and ion exchange. However, the majority of these techniques are complex, highly sensitive to environmental factors, expensive, take longer to complete, and produce hazardous by-products (Cojocariu et al. 2018).

The most recently developed method, “*phytofiltration*,” is used in this study to extract harmful and dangerous dyes from water using plant-based materials. This method is being studied extensively since the raw materials (agro waste) are often inexpensive, readily available, simple to utilize, and environmentally benign for eliminating any kind of pollution from water. The reason this technology is so popular is that the raw materials (agro waste) used to remove all kinds of impurities from water are often inexpensive, readily available, easy to use, and environmentally acceptable. Agro wastes such as pine cone treated with nitric acid (Gören et al. 2021), peeling of watermelon as well as water chestnut treated with citric acid (Hussain et al. 2021a) and *Dalbergia sissoo*-activated carbon (Shrestha 2021) had

provided efficient adsorptive removal results for RAD in earlier studies. So, we explored *Trapa natans* (Chestnut) (Mendhekar and Rachh 2023) peels in this work for phytoremediation of persistent organic pollutants, like dyes. They are extensively found in arid and humid environment during rainy and cold seasons. They are widely used in food, herbal medicines (Banu et al. 2023). They are reported earlier for removal of Cr(VI) (Kumar et al. 2020), Ni(II) (Mukhlis et al. 2023), As(III), brilliant green (Rehman et al. 2016), amaranth (Singh et al. 2020), acid violet (Rehman et al. 2024), and dyes (Khan et al. 2013).

Researchers found that, in comparison to its raw and untreated counterparts, the chemically processed biosorbent had demonstrated good and promising performance. An inexpensive, environmentally benign, plentiful, and easily accessible agro waste TP was selected to remove dangerous and toxic RAD from wastewater, based on previously published results of dye phytofiltration. By providing more active binding spots for adsorption during contact with the dye molecules in wastewater, the primary goal of this study is to modify the surface morphology of lignocellulose biomass. The adsorbents' ability to extract dyes from water will increase along with their speed of action, after being treated with the best modifying agent. The aim of this research is to assess the phytofiltration performance and effectiveness of the chosen biosorbent for the eradication of dyes under appropriate circumstances by chemically modifying them with various chemicals (solvents and chelating agents).

Supplies and methods

Chemicals

Throughout this study, pure solvents and compounds are hydrochloric acid (37%, 11.6 M), some organic acids: propanone, (R-OH) methyl, ethyl, and isopropyl alcohols, sodium hydroxide, sodium carbonate, potassium iodide, iodine, indicators, and sulfuric acid. Chelating substances such as lactic acid as well as tartaric acid were obtained from trusted and well-known companies, Merck and Fluke. Rhodamine-B dye (λ_{\max} : 554 nm), crystals containing iodine (99.8%) across organics, NaHCO₃, CaCO₃, NaCl, KCl (Friends Laboratory Chemicals), FeCl₃, zinc chloride (Merck), lead nitrate (Riedel-de-Haen). Before being used, the glassware was sterilized in an electric oven at 70 °C for 30 min after being cleaned with an H₂CrO₄/H₂O solution.

Instrumentation

Rhodamine-B samples were investigated via a UV–visible spectrophotometer (CECIL CE-7200) at λ_{\max} : 554 nm. A pH meter with digital readings was employed to determine

the pH of different liquids. Samples were agitated in a batch manner using an automated shaker.

Methodology for setting up raw biosorbent

The decision to use water chestnut peel as the sorbent material was based on the material's abundance, undervaluation, and eventual disposal as agricultural waste.

Trapa natans (TP) was purchased from Lahore and the surrounding regions. The peels were then cleaned under running water to get rid of any waste materials and trapped dust. After carefully cutting the peels of both adsorbents into sizes appropriate for the tests with a sharp knife, they were thoroughly cleaned with purified water. Afterward, the peels were set out in the sun for eight days and then baked at around 70 °C for seventy-two hours in order to extract the moisture that had been contained during the first stage. After crushing, water chestnut peels were processed to a size of 70 mesh, producing a fine powder. To eliminate any remaining moisture that had been caught during the second phase, these chopped peels were once more baked to dry for a full day. They were then put in plastic jars marked TP in preparation for adsorption experiment research (Hussain et al. 2022a). Schematic diagram for preparation of raw adsorbent is explained in Fig. 1.

The dye's determination

In order to create the concentration of 1000 ppm, 1.0 g of RAD was first dissolved in a tiny amount of water and then filled off with 1000 mL of distilled water. Using the

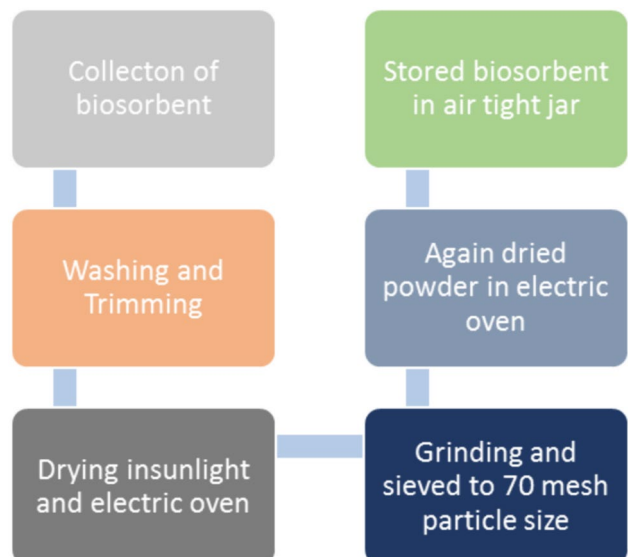


Fig. 1 Diagram showing the steps involved in making natural adsorbent

CECIL CE-7200 spectrophotometer, standards with concentrations between 10 and 50 ppm were prepared from this stock solution, and their absorbance was measured. The calibration curve was used to calculate the concentration of each dye in the solution both before and after sorbent was added. This enabled researcher to calculate the effectiveness of each sorbent material in terms of dye removal.

Characterization of biomaterial

Several methods were used to examine TP, including particle density, iodine titration, pH, proportion of ash and moisture content, volatile matter measurements, calculation of porosity/bulk density, and elemental analysis listed in Table 1.

For the determination of moisture content of adsorbent, a thermal drying method was used. Two grams of adsorbent was weighed and placed in washed pre-weighed crucibles. The crucible was placed in oven and dried to a constant temperature of 80 °C for 4 h. The percentage moisture content was then calculated using a formula:

$$\text{Moisture (\%)} = \frac{\text{loss in weight on drying the adsorbent}}{\text{initial weight of the adsorbent}} \times 100 \quad (1)$$

A stock solution was made by taking 2.7g of iodine crystals additionally 4.1g of potassium iodide in a 1000-mL measuring flask, then diluting it up to the mark with distilled water. Utilizing a standard sodium thiosulfate liquid (0.1 M), this stock solution was standardized. 0.5g of the adsorbent and 10mL of 5% v/v HCl were taken in a 100-mL measuring flask. The flask was shaken so that the adsorbent was wetted. 100 mL of stock solution of iodine was added to HCl solution and agitated at a fast rate for a period of 60 min using an orbital shaker. A small portion of the sample (10 mL) was titrated with a standard solution of 0.1M sodium thiosulfate to make use of the starch solution as an indicating reagent. The amount of iodine adsorbed in milligrams was used to calculate the

iodine amount that the adsorbent will take up at ambient temperature.

$$\text{Iodine Number} \left(\frac{\text{mg}}{\text{g}} \right) = \frac{(B - S)}{B} \times \frac{V \times M}{W} \times 253.81 \quad (2)$$

B is the amount of sodium thiosulfate needed in the titration blank. 'S' stands for the amount of sodium thiosulfate needed in the sample solution. 'V' indicates the volume taken (10 mL). M is the molarity of sodium thiosulfate. 'W' signifies the adsorbent's mass and the molar mass of iodine (253.81).

Weighing a density bottle with a lid (W_i), following that we weighed once again to determine the bulk density of U-TP (W_p) after its filling with distilled water, removing the (W_i) from the (W_p) yielded the mass of water. Equation (1), whereby water mass is difference obtained and its density is 1 g/cm³ at room temperature. Subsequently, a precise quantity of every sample was extracted and placed in a density container, after which its volume was determined by reweighing. The bulk density of U-TP was calculated using Eq. (5).

$$\text{Density} = \frac{\text{mass of wet sample}}{\text{volume of water in bottle}} \quad (3)$$

$$V = d \times W \quad (4)$$

$$\text{Bulk density} = \frac{\text{mass of wet sample peels}}{\text{volume os sample peels}} \quad (5)$$

in which V_v is the void volume, and V_t is total volume. Following relationship was used to determine each adsorbent's volumes and porosity:

$$V_s = \frac{Ms \times dw}{Gs} \quad (6)$$

$$\text{Porosity} = \frac{\text{Volume of voids } (V_v)}{\text{Total volume of cylinder } (V_t)} \quad (7)$$

$$\text{Void volume } (V_v) = V_t - V_s \quad (8)$$

'Ms' is specific mass of cylinder, 'dw' is density of water, 'Gs' is specific Gravity.

2.0 g adsorbent was placed in a washed, dried, and pre-weighed crucible. The crucible was then placed in an electric furnace and the temperature was maintained at 500 °C for 8 h. Then the adsorbent was allowed to cool at 30 °C and the weight was noted again. The ash contents were determined (Mahmud et al. 2021) and % of volatile matter (Nsubuga et al. 2021) using the following expression:

Table 1 Physiochemical characterization of U-TP

Property	U-TP
Particle density	0.640g/cm ³
Bulk density	0.48 g/cm ³
Porosity	35.79%
Moisture	85%
Ash	5%
Volatile matter	95%
Iodine number	30.65mg/g

$$\text{Ash (\%)} = \frac{\text{ash weight}}{\text{initial dry weight}} \times 100 \quad (9)$$

$$\text{Volatile matter (\%)} = \frac{\text{weight of volatile compound}}{\text{initial dry weight}} \times 100 \quad (10)$$

Elemental analysis was done with AAS using acid digestion method of samples, and results are given in Table 1.

Treatment of biomass

In first phase, chemical processing is done by decolorizing with hydrogen peroxide. For this purpose, Erlenmeyer flasks sealed with aluminum foil were filled with 100 g biosorbent and solvent 250 mL. The mixture was agitated for six to ten hours at 30 °C at 140 rpm. In order to prevent the native adsorbents from deteriorating, extra and excessive exposure in solvent-based altering agents was prevented in alkali and acidic conditions. To get rid of any trapped solvent molecules, the contents of each flask were properly filtered and cleaned with distilled water. This decolorized biomass was then preserved in plastic jars for further treatment after being dried in an electrically heated oven at 80 °C for 24 h.

In second phase, using a chelating agent, solid-state chemical alteration is accomplished. It was performed using various chelating agent in order to enhance the extra locations of active adsorption binding on the surfaces of both untreated (U-TP) and treated biosorbent (T-TP). In order to do this, 5 g of each chelating agent and 100 g of powdered biosorbent TP were well mixed in separate china dishes. After covering each china dish with aluminum foil, it was microwave-heated for eight to ten minutes. In order to facilitate future research, acidic modified adsorbent was carefully preserved in plastic jars. In a batch mode study, the chemically modified adsorbent was evaluated for the withdraw of dye from water bodies under suitable conditions for use (Heba et al. 2019).

Experiment in Biosorption research

Using the tartaric acid-treated new adsorbent, the maximal adsorptive removal of basic dyes (RAD) in the batch mode studies was encouraging. The native TP was designated as T-TP for additional research following chemical treatment and modification. To optimize the operational parameters for adsorption experiments, 25 ppm of each RAD solution was created throughout the experimental method, and 100-mL conical flasks were filled with 25 mL of each solution. The fundamental (cationic) model dyes' chemical structures were chosen in order to remove them from wastewater. The

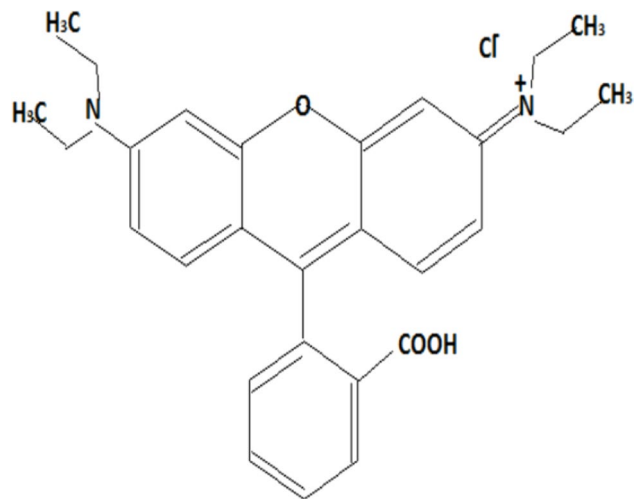


Fig. 2 Chemical structure of RAD

chemical structure of RAD is shown in Fig. 2 (Soylak et al. 2011).

Optimization of Biosorption conditions for RAD

The target quantity of 25 ppm was achieved by diluting a stock solution of dye. In order to investigate the effects of pH (1–10), temperature (20–80 °C), shaking speed (60–140 rpm), biosorbent dosage (0.2–2 g), contact time (10–100 min), and starting dye concentration (5–50 ppm), batch adsorption tests were carried out. In each experiment, a conical flask holding 25 mL of dye solution is being filled, and 0.5 g of adsorbent was combined with it. A mechanical shaker was used to shake the solution. At λ_{max} 554 nm, the adsorption of dye onto peel powder was examined via a UV spectrophotometer (Mittal et al. 2013).

The % removal of dye by using tartaric acid-modified adsorbent was determined through following equation (Rehman et al. 2011):

$$\% \text{Removal of dye} = \left(\frac{C_o - C_e}{C_o} \right) \times 100 \quad (11)$$

The quantity adsorbed per unit mass of adsorbent (Q), also known as the adsorption capacity, was determined using Eq. (12) (Vinod et al. 2012):

$$Q = \frac{(C_o - C_e)V}{W} \quad (12)$$

where C_o and C_e are the initial and t-time (in ppm) concentrations of RAD in solution, respectively. The mass of adsorbent is m (g), and volume of dye solution is V (L).

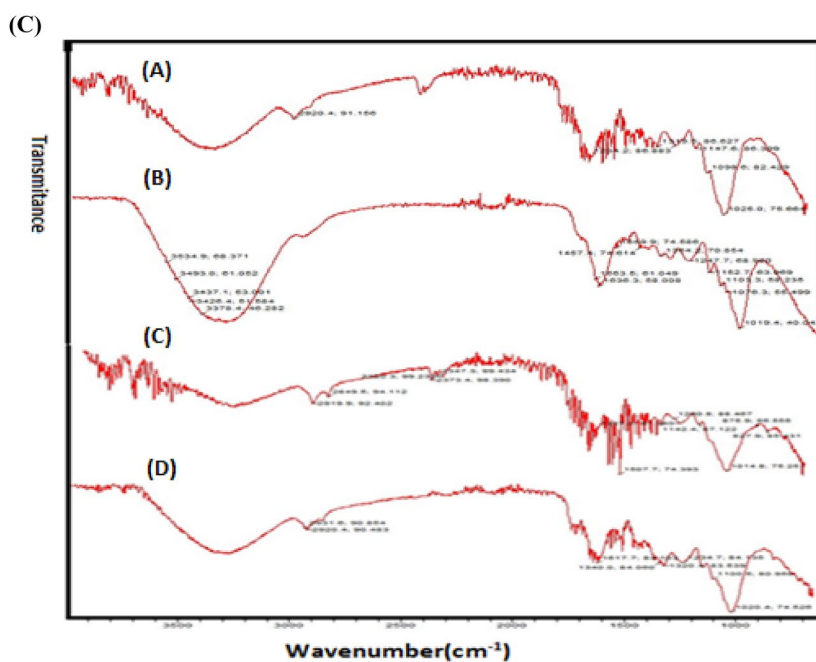
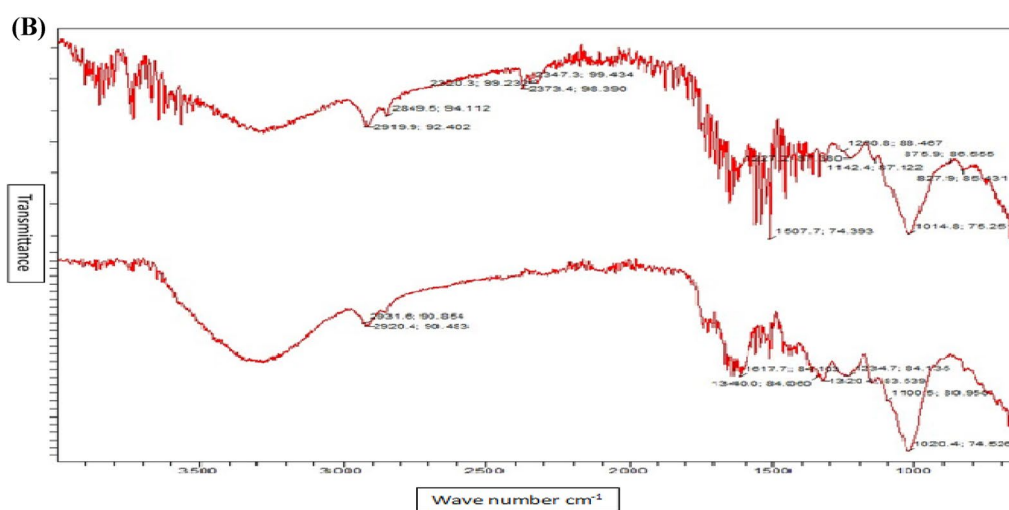
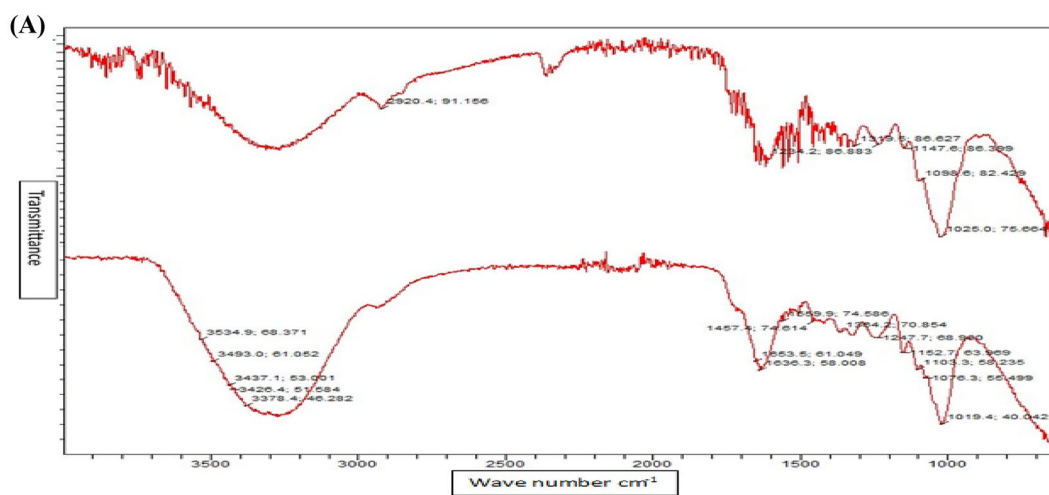


Fig. 3 **A** Comparisons of FT-IR analysis of raw (U-TP) and tartaric acid-modified (T-TP) *Trapa natans* peels before adsorption. **B** A comparison of FT-IR analysis of untreated (U-TP) and tartaric acid-treated (T-TP) *Trapa natans* peels after adsorption of RAD. **C** Comparative analysis of before and after adsorption of RAD

Results and discussion

After many experiments, the most suitable modifying agent was selected for the alteration of TP's surface morphology. The FT-IR method was used to characterize the adsorbents. Using kinetics modeling, Freundlich, Temkin, Langmuir, and equilibrium data, the data's credibility and dependability were evaluated.

Chemical modification of biomass

A range of substances, including various organic solvents, acids, chelating agents, and alkalis, was used to chemically treat the raw biosorbent TP. For the purpose of removing RAD from the water system, the adsorption ability of chemically treated biosorbent with various compounds was evaluated. The surfaces of biosorbent have been esterified with OH groups to form tartaric acid, as demonstrated by FT-IR measurement, and this has created an increasing number of binding sites for it to bind using contaminant molecules extracted from water. Consequently, improved locations of active binding on the surfaces of treated biosorbent were facilitated rapid and effective adsorption equilibria at the adsorbate–adsorbent interface.

When compared to other chemicals used, the maximal adsorptions of RAD on the untreated and tartaric acid-modified adsorbents U-TP and T-TP under optimized circumstances were determined to be 91% and 96%, respectively. Under microwave irradiation, raw biosorbent (U-TP and T-TP) underwent solid phase chemical modification.

Spectroscopic analysis

FTIR analysis before adsorption

Study of comparative FT-IR analysis of U-TP and T-TP before adsorption is illustrated in Fig. 3A. At 30 °C with 125 rpm for 20 min, 0.5 g of each U-TP and T-TP was individually added to two conical flasks holding 25 mL RAD solutions with a 25 ppm concentration. Each sample underwent filtering and. For FT-IR analysis, the left-over material was dried following adsorption. A contrast analysis of water chestnut peels in their original state (TP) and after chemically treating them with tartaric acid (T-TP) is shown in Fig. 3A and Table 2. The surface alteration resulting from esterification on modulating agent (tartaric acid) between the free OH groups of alcohols was seen in the range between

3500 and 3300 cm^{-1} which were not in U-TP. A broad band in range of 3300–3500 cm^{-1} displayed the COOH moieties on *Trapa natans*, which was changes after treatment C–O stretching vibrations range in UTP and TTP is 1319.5 cm^{-1} and (1100–1300) cm^{-1} , respectively. As a result, the TP-modified spectra contained high concentration of carboxylic acid groups to enable effective as well as rapid adsorption of certain dyes.

Study of FTIR after adsorption

Figure 3B compares peels of *Trapa natans* in their original form (U-TP) with after chemically treating them along with tartaric acid (T-TP) following the adsorption of RAD. The region between 1000 and 1300 cm^{-1} that was not in U-TP was where the surface modification brought about by esterification of alcohols between their free OH molecules on the modulating agent tartaric acid was seen. Peaks 1617.7 cm^{-1} and 1320.04 cm^{-1} most probably represented the carboxylic group T-TP. Because of this, the TP-modified spectra had an increasing number of carboxylic acid groups, which made it possible for certain dyes to adsorb quickly and efficiently. Better binding with cationic dye will result from the increased oxygen in functional groups (RAD).

Comparative analysis of before and after adsorption

All FTIR spectra of model dye RAD depicted in Fig. 3C are graphs of (UTP and TTP) before and after adsorption of RAD. Treated biomaterials show more adsorption as compared to untreated ones. The change in wavenumber at (3534.9, 3493.0, 3437.1, 3426.4, 3378.4) cm^{-1} in Fig. 3B and 2931.6, 2920.4 and 1617.7, 1320.4 in Fig. 3C shows significant intermolecular interactions between RAD and tartaric acid-modified adsorbent. It was concluded from earlier reported data the oxygen-containing functional group enhances cationic dye adsorption. Comparison of FTIR peak values is explained in Table 2.

SEM analysis

Surface analysis of biomass was done with SEM–EDX, and results are reported in Fig. 4. As it is evident from Fig. 4A that untreated adsorbent surface is comparatively smooth with less exposure of binding sites, which becomes more evident in Fig. 4A-b after microwave-assisted tartaric acid treatment. These sites were covered with RAD after adsorption predicting that physisorption mode of biosorption also enhances after chemical treatment along with chelating ability of biomass for phytofiltration of dye.

Table 2 Comparison of FTIR value of before and after adsorption of RAD

Functional group	Ranges in IR spectrum(cm^{-1})	Before adsorption (cm^{-1})	After adsorption (cm^{-1})
<i>Untreated biomaterial</i>			
C–H Stretching	2800–3300	2920.4	2931.6
C–C Stretching	1200–1600	1025.0	1020.4
C–O stretching	1000–1300	1319.5	1320.4,1340.0,1234.7
<i>Treated adsorbent</i>			
O–H	3200–3600	3534.9,3493.0,3437.1,3426.4,3378.4	
C–H Stretching	2800–3300		2931.6,2920.4
C=O carboxylic	1600–1800 (FGR) Lessthan1500(FPR)		1617.7,1320.4
C–H bending	500–1500	1457.4,1384.2,1019.4	
C–C Stretching	1200–1600	1384.2	
C–O stretching	1000–1300	1247.7,1152.7	1340,1234.84,1100,1020

EDX analysis

It indicated that no harmful moieties and metal ions are present in *Trapa natans* peels before and after chemical treatment and neither after removing RAD, so it is safe to use for phytofiltration of dyes on larger scale.

Effective conditions for phytofiltration of RAD by biosorption

In order to determine the pH, 200-mL flasks containing 1 g of water chestnut peels' powder were each filled with 40 mL of deionized water and continuously swirled for an hour. After the sample mixes stabilized, a pH meter was utilized for measuring the pH (Zango and Imam 2018). The point of zero charge (pH_{pzc}) has been used in acid–base titrations to determine the net surface charge of adsorbent materials. Ten Erlenmeyer flask sets, each with a pH label (1 to 10), were filled with 200 mL of a 25 ppm sodium chloride solution and 0.5 g of TP individually to identify point of zero charge. Using a pH meter and solutions of NaOH and HCl, initial pH of each solution was altered. Using a pH meter and solutions of NaOH and HCl, the starting pH of each solution was changed. Each sample's ultimate pH was measured at 30°C after 10 h. After that, difference in pH change between the first and final readings was used to visually assess the point of zero charge. The negatively charged adsorbent surfaces are where the basic dye cations are more selectively bound and likewise if $\text{pH}_{(\text{adsorbent})} > \text{pH}_{\text{pzc}}$ (Kabir et al. 2022). This indicates that the surface of the adsorbent is more strongly negatively charged. Results from pH_{pzc} support the observation made via chemical composition, moisture absorption, surface tension, and morphological investigations (Wang et al. 2020) that chemical treatment significantly altered the surface. Figure 5 shows variation of (A) pH_f vs pH_i and (B) ΔpH vs pH_i . The graphic representations of ΔpH vs. pH_i

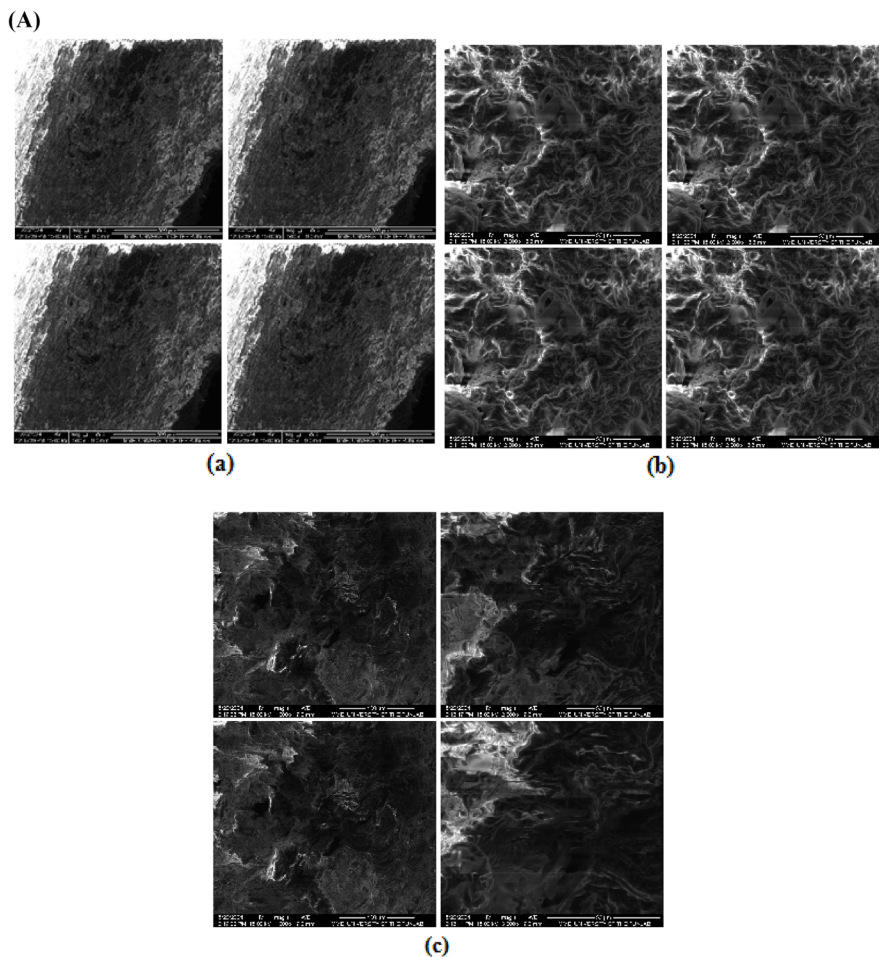
in Fig. 5A, B complement one another and make it simpler to examine and comprehend how the charge distribution depends on the surfaces of the adsorbents. As a result, Fig. 5A demonstrates that both adsorbent UTP and TTP had a similar pattern, however with notable variations in the absolute values, making it feasible to see that the pH_f varies more than the pH_i within a certain range (2–10). As seen in Fig. 5B, the pH_{ZPC} values for UTP and TTP were 6 and 4, respectively. According to Fig. 5B, the ΔpH values for UTP increased up until $\text{pH}_i = 10.0$. This behavior makes sense given UTP, where hydroxyl-containing compounds like cellulose, hemicellulose, and lignin can encourage protonation, raising pH_f and ΔpH values and encouraging the development of positively charged surfaces ($\text{pH}_i < \text{pH}_{\text{pzc}}$) (Anfar et al. 2020). The same tendency is seen for TTP, as shown in Fig. 5(B), increasing the exposure of the cellulose's hydroxyl groups due to the reduction of steric hindrance (Ferreira and Taherzadeh 2020); a negatively charged surface may be produced throughout a wide pH_i range by the increased availability of hydroxyl groups that can undergo deprotonation at low pH_i values ($> \text{pH}_{\text{pzc}}$) and generate an electrostatic attraction. The findings shown in Fig. 5A, B can be highly helpful in understanding the variations in the kinetic and thermodynamic parameters, removal efficiency, and adsorption capacity that are involved in RAD removal.

Using untreated and tartaric acid-treated biomaterial, the optimal conditions for adsorptive eradication of RAD were found by adjusting parameters, such as: temperature, dosage of the biosorbent, time of retention, rate of stirring, and solution pH.

Effect of agitation speed

Because it causes a thin layer of adsorbate (RAD) to develop on adsorbents from solutions, it is an important component that regulates the adsorption behavior. Adsorption efficiency

Fig. 4 **A** SEM analysis of (a) raw *Trapa natan* peels before adsorption, (b) treated *Trapa natan* peels before adsorption, (c) treated *Trapa natan* peels after adsorption of RAD. **B** SEM analysis of (a) raw *Trapa natan* peels before adsorption, (b) treated *Trapa natan* peels before adsorption, (c) treated *Trapa natan* peels after adsorption of RAD



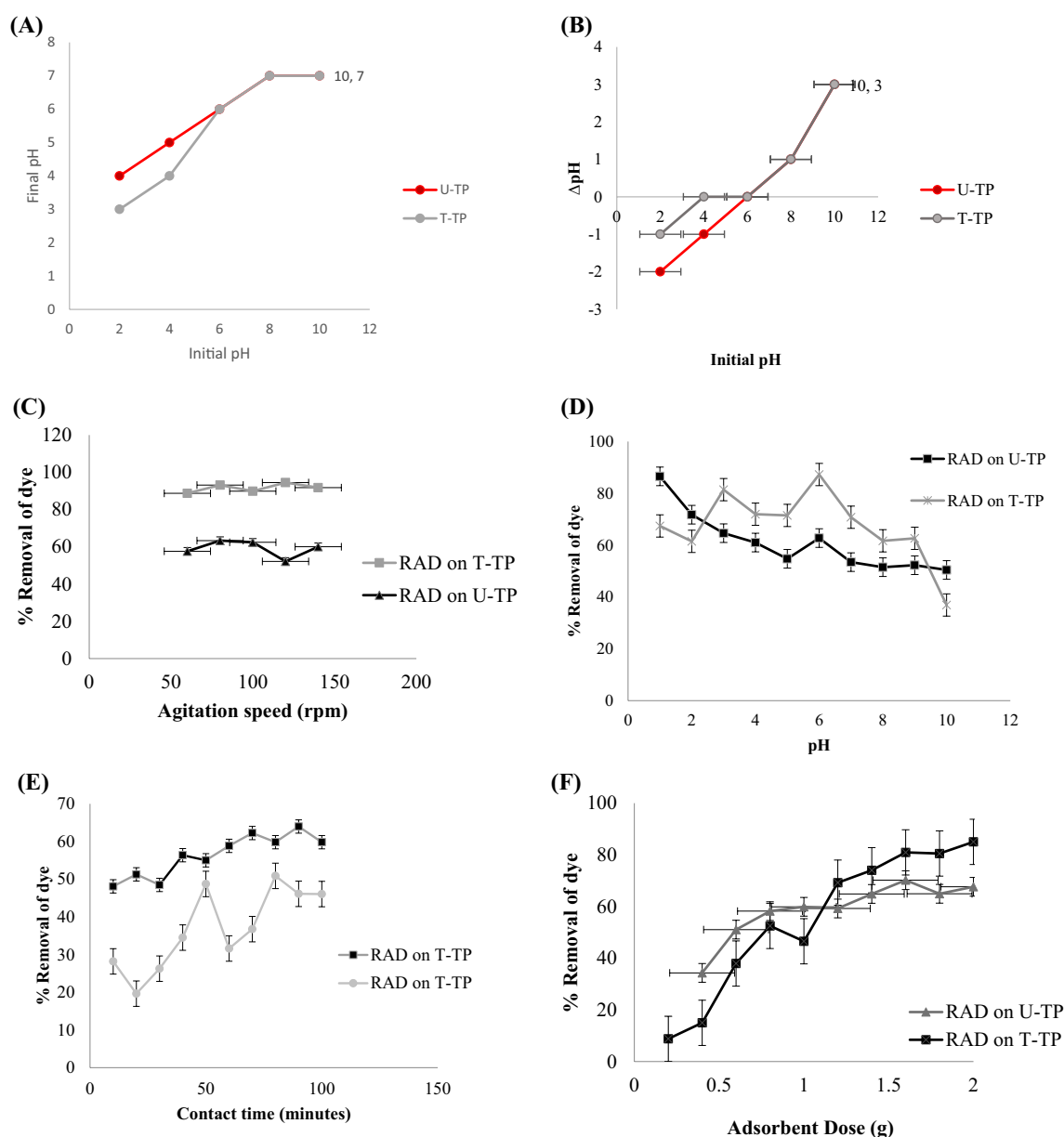


Fig. 5 **A** Variation of pH_f vs pH_i . **B** Variation of ΔpH vs pH_i . **C** Agitation speed's impact on removal of RAD. **D** The impact of pH variations on removal of RAD. **E** Effect of change in contact time on removal of RAD. **F** Effect of change in adsorbent dose on removal of RAD

is enhanced and promoted when cationic dye molecules on modified adsorbents form a unique and distinct outermost border. Thus, on using U-TP T-TP, agitation rate affected RAD adhesion. This factor was examined at speeds between 60 and 140 rpm, with a little 20 rpm variation. Other suitable operating conditions, such as a contact period of 20 min, 25 °C as the temperature, 0.5 g of the adsorbent dose, and a concentration of 25 for each dye solution, were also used in the batch mode experiments.

As a result, as Fig. 5C illustrates, the maximum adsorptive reduction RAD on U-TP and T-TP was 63.67 and 94.49% at 80 and 120 rpm agitation speed, respectively. As

demonstrated in Fig. 5C, high speed was associated with a reduction in the process of adsorption during the experiment due to the production of an overly independent RAD molecules flowing at a constant circular velocity in water (Mohapi et al. 2020).

Effect of pH

During the experimental work, using 0.1 M NaOH or 0.1 M HCl solutions, the pH of the dye adsorption on lignocellulose surfaces was adjusted during the experiment. The pH_{PZC} of biosorbent U-TP and T-TP, which was experimentally

found to be 6 and 4, respectively, is important for assessing respective capacities for adsorption of model dye. Figure 5D shows how pH affects the adsorption of dye on U-TP and T-TP. To conduct smooth experimental studies, two sets of Erlenmeyer flasks with a volume of 25 mL each were used to collect 25 ppm solutions. Each set contained ten flasks. Each set contained 0.5 g of each U-TP and other set T-TP, respectively. When pH was equal to 1, the highest adsorption of RAD on U-TP was 86.56%, whereas on T-TP, it reached 87.26% at pH 6. As the pH is increased, there is a decrease in the hydrogen cations, so the adsorbents' charge becomes negative, the material promotes the adsorption of dye cations through electrostatic attraction. In case of U-TP $\text{pH} < \text{pH}_{\text{PZC}}$ so the adsorption take place is because of COO^- and H^+ attraction at low pH but on contrary $\text{pH}_{\text{PZC}} < \text{pH}$ which increases the negative ion and attract dye cation (Benjeloun et al. 2022).

Figure 5D further demonstrates how an increase in pH was linked to a decline in RAD's adsorption efficiency. This, in turn, affected equilibrium forming with adsorption interaction active sites [COO^-] on the biosorbent U-TP and T-TP surfaces, as well as the appealing connections between free [OH^-] ions with [RAD^+] cation in the water-based solution, which blocked their ability to reach their negatively charged spots for adsorption on the biosorbent surfaces.

Impact of duration of contact

Regarding the biosorbents U-TP and T-TP interactions, as illustrated in Fig. 10, the quantity of binding sites that are available and contact time interval are connected to the adsorption process's performance. Before declining by unit mass as a result of equilibrium being established and a large number of unoccupied adsorption binding regions that are still present on the U-TP and T-TP surfaces, at initial stage the adsorption of RAD increased with a longer

contact period until ideal time interval was reached. In order to establish a contact time duration of 10–100 min with a deviation of 10 min, this experiment employed 25 mL of each of the RAD solutions at a concentration of 25 ppm.

Figure 5E shows optimal interval for the highest percentage of RAD adsorption removal on U-TP, 63.98% at 90 min. At 80 min, the adsorptive elimination of RAD from an aqueous solution on T-TP was 50.88%. Table 3 illustrates the encouraging efficiency of U-TP and T-TP's adsorption performance in comparison to previously published data, due to RAD's susceptibility to intraparticle diffusion and additional adsorption sites that are active.

Furthermore, excess of RAD positive charges on the surfaces of U-TP as well as T-TP causes a decrease in the effectiveness of the adsorption performance as time passes after the ideal time interval.

Effect of dosage of adsorbent

U-TP and T-TP adsorbent doses varied from 0.2 to 2.0 g, fluctuating by 0.1 g used in various operating situations. The FT-IR interpretation indicates that the adsorbents U-TP and T-TP, include extra COOH groups, have a higher binding affinity on their interfaces for the cationic dye molecules RAD^+ . For this investigation, two sets of Erlenmeyer flasks, each containing ten flasks for smooth experimental investigations, were used to hold different 25 ppm solutions with a volume of 25 mL. The following experimental operating parameters were used for the determination of adsorption dose:

Temperature of 30 °C, agitation speed of 125 rpm, for RAD on U-TP and T-TP. The experimental findings are graphically shown in Fig. 5F. There was a maximum RAD adsorptive removal of 70.189 percent for U-TP in 0.5 g with 85.108 percent for T-TP (0.5 g) from aqueous solution. Additionally, Fig. 5F shows that model dye's adsorption,

Table 3 A comparison of adsorption capacities of RAD with reported biomaterials

Biosorbent	Adsorption capability (mg/g)	References
Pomegranate peels	30.47	Ghibate et al. (2021)
Raw Plantain Peel	16.57	Adeleke et al. (2023)
Groundnut seed cake powder	18.2	Kumar et al. (2023)
<i>Oryza sativa</i> ash	250	Dutta et al. (2014)
<i>Elaeis guineensis</i> shell	108	Zhi and Zaini (2019)
Waste cassava slag	105.3	Wu et al. (2020)
Paper industry waste sludge	6.711	Thakur and Kaur (2016)
<i>Gracilaria edulis</i>	8.96	Selvakumar and Rang-abhashiyam (2019)
<i>Artocarpus heterophyllus</i> seed	26.4	Nascimento et al. (2021)
Walnut shell treated with acrylic acid	48.87	Guo et al. (2023)
Citric-acid-modified <i>Trapa natans</i> peels	15.63	Hussain et al. (2022a)

including RAD, rises at low concentrations because there are more binding sites accessible. However, when concentration rises, a rapid equilibrium is reached at the interfaces between adsorbate and adsorbent, which reduces adsorption. For additional experimental research, an adsorbent dosage of 0.5 g was shown to be the best one.

Study of isothermal and kinetic models of Biosorption procedure

Method for equilibrium isothermal model development

To evaluate the validity and reliability of the experiments conducted for the adsorption of dye on simple and tartaric acid-modified biosorbent (U-TP along with T-TP), four isothermal models were linked together and applied using linear Eqs. (13), (15), (16) and (18), respectively, to evaluate the accuracy and veracity of the experiments carried out for the dye adsorption on simple and tartaric acid-modified biosorbent (U-TP, T-TP). The following ideal parameters were used to conduct the biosorption

investigation: The starting volume and concentrations of each solution were 100 mL and 25 ppm. There were 90- and 120-min intervals between contacts. Adsorbent dosage was 1.4 g and 2 g. The temperature was 50 and 80 °C. The agitation speed was 80 and 120 rpm for U-TP and T-TP, respectively.

(1) The Langmuir Isotherm

According to the Langmuir model, monolayer adsorption occurs on a uniform surface that has a limited quantity of adsorption sites and very little mutual contact between the molecules that have been adsorbed. The Langmuir isotherm model is expressed as a linear regression in Eq. (13), and effective graphical components are explained in detail in Fig. 6A:

$$\frac{1}{Q_e} = \left(\frac{1}{bQ_{max}} \right) \frac{1}{C_e} + \left(\frac{1}{Q_{max}} \right) \quad (13)$$

Here, " Q_i " denotes the amount of RAD adsorbed in parts per million (ppm), " C_e " is the residual amount, and " Q_{max} " denotes the highest possible adsorption level in

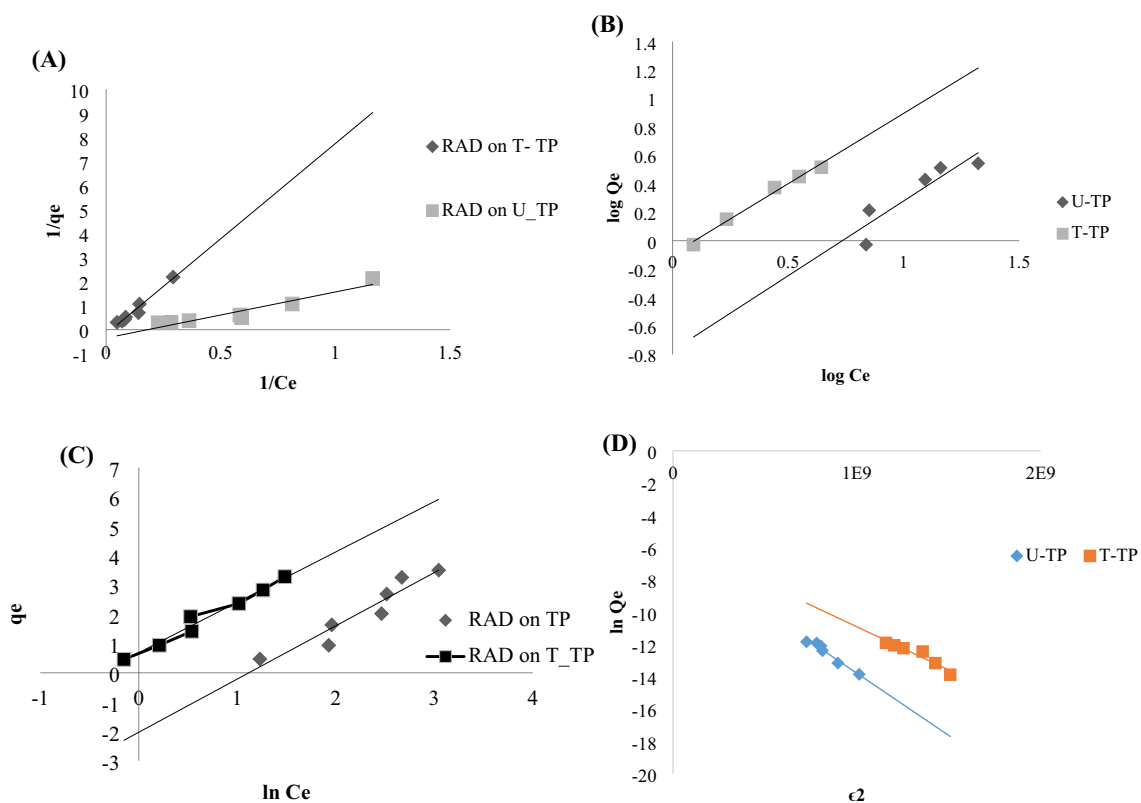


Fig. 6 **A** Comparing the removal of dye effectiveness of simple and tartaric acid-modified biosorbent using the Langmuir isothermal model. T-TP is a treated adsorbent, whereas U-TP is an untreated one. **B** Assessment of dye removal effectiveness of simple (TP) and tartaric acid-modified (T-TP) biomaterials using the Freundlich model. **C** An analysis of the Temkin isothermal model comparing acid-

treated biosorbent' adsorptive dye removal performance. Adsorbents U-TP and T-TP are untreated and treated, respectively. **D** An analysis of the DR isothermal model comparing acid-treated biosorbent' adsorptive dye removal performance. Adsorbents U-TP and T-TP are untreated and treated, respectively

milligrams per gram (mg g^{-1}), and "b" denotes the adsorption capacity (L/g).

The dye's adsorption on U-TP has a correlation coefficient (R^2) of 0.9079, but on T-TP it was 0.9708. The Langmuir model fits the adsorption performance of U-TP and T-TP in this study the best, as indicated by the values of " R^2 " being almost equal to unity in every instance. For RAD adsorption, the maximum adsorption capacity (Q_{\max}) on U-TP was 2.8801 mg/g , while on T-TP, it was 5.5803 mg/g . The following formula was used to get the separation factor (R_L):

$$R_L = \left(\frac{1}{1 + bC_0} \right) \quad (14)$$

The R_L value represents the adsorption nature either unfavorable ($R_L > 1$), linear ($R_L = 1$), favorable ($0 < R_L < 1$), or irreversible ($R_L = 0$). The Freundlich isotherm model was applied to the non-ideal, multilayer adsorption on heterogeneous adsorbent surface. Its number, which falls between "0 and 1," indicates a decent adsorption rate. For the adsorption of RAD on U-TP, the separation factor (R_L) was 0.1552, while for T-TP, it was 0.5974. These results, which are less than "1," show a decent rate of adsorption and demonstrate how well the Langmuir model for biosorption has been applied. The monolayer homogeneous adsorption of dyes on U-TP and T-TP at a particular number of identical adsorption binding sites dispersed on the interface borders of both biosorbents is further shown by " Q_{\max} " values.

(2) Freundlich Isotherm

The surface heterogeneity of U-TP and acid-modified adsorbents T-TP, as well as their activity for adsorption performance toward RAD in aqueous solutions, is assessed using the Freundlich isothermal model. It is focused on how energy is distributed differently during physisorption and chemisorption. This isothermal system's linear trend is represented by Eq. (15) (Geçgel et al. 2013).

$$\ln q_e = \left(\ln K_F + \frac{1}{n} \ln C_e \right) \quad (15)$$

Figure 6B presents a graphical comparison of the Freundlich model [$\ln Q_e$ against $\ln C_e$], showing straight lines for each of the biosorbent (U-TP as well as T-TP). Here, " K_F " ($\text{mg}^{1-1/n} \text{L}^{1/n} \text{g}^{-1}$) is the binding factor, while the adsorption frequency is represented by "n." Figure 6B presents a graphical comparison of the Freundlich model [$\ln Q_e$ against $\ln C_e$], showing straight lines for each of the biosorbent (U-TP as well as T-TP).

According to Fig. 6B graphical depiction, RAD correlation coefficient values on U-TP along with T-TP, each model dye's slope ($1/n$) was less than 1, which suggests the variety of adsorption sites on the interface of U-TP's as well as T-TP's with adsorption capacity, were: 0.8552 and 0.8832, respectively. For sportive removal of RAD on U-TP

and T-TP, the correlation coefficients (R^2) were: 0.8291 and 0.9883, respectively, indicating that physisorptive removal of RAD increased after chemical treatment of peels with tartaric acid. Compared to other models, the Langmuir model is the most favorable as indicated from Table 4.

(3) Temkin isotherm

Based on the fundamental premise, Temkin model suggests a roughly equal dispersion of affinity for binding in U-TP and T-TP. Consequently, when RAD molecules saturate binding locations on adsorbent surfaces, thermal diffusivity progressively drops. The following equation displays the Temkin isotherm's linear representation:

$$q_e = (B_T \ln K_T + B_T \ln C_e) \quad (16)$$

The energy emitted through adsorption is denoted by the Temkin isotherm constant, $B_T = RT/bT$ (kJ/mol), while the equilibrium binding constant " K_T " (L/g) represents the highest binding energy. A graph was plotted for analysis of Temkin isotherm model in Fig. 6C.

Equation (16) for adsorption of dye on U-TP as well as T-TP was used to calculate these constants throughout experimental investigation using linear regression of the graph with " C_e and $\ln C_e$ " in between as seen graphically in Fig. 6C. Table 5 displays the Temkin isotherm parameters.

The heat of adsorption (B_T) for dye on U-TP and T-TP found to be 1.8147 kJ/mol and 1.7175 kJ/mol , respectively. The adsorbate-adsorbent interactions are confirmed to be weak and physical when the B_T findings are less than 8, indicating physisorption as opposed to chemisorption. For Temkin model, R^2 values were lower than those of the Freundlich or Langmuir isothermal systems, indicating an inadequate match between

Table 4 An analysis comparing isothermal conditions for RAD removal from untreated and treated adsorbent

Parameters	RAD on U-TP	RAD on T-TP
<i>Langmuir Isotherm adsorption model</i>		
R^2	0.9079	0.9708
Q_{\max} (mg/g)	2.8801	5.5803
R_L	0.1552	0.5974
b (L/mg)	0.1814	0.0226
<i>Freundlich isothermal adsorption model</i>		
R^2	0.8291	0.9883
n ($1/m$)	0.8552	0.8832
<i>Temkin isotherm adsorption model</i>		
R^2	0.9032	0.9734
K_T (L/g)	3.0583	1.4914
B_T (kJ/mol)	1.8147	1.7175
<i>Dubinin-Radushkevich adsorption model</i>		
Q_m	0.002343288	0.003826518
E	7.91E+03	1.00E+04

Table 5 Investigation of kinetic equilibrium models in comparison

Parameters	U-TP	T-TP
<i>Assessment of first-order pseudo-kinetics</i>		
R^2	0.4752	0.7594
Q_e (mg/g)	4.91553	6.90192
K_1 (g/mg ⁻¹ min ⁻¹)	-0.0001	-0.0002
<i>Assessment of pseudo-second-order kinetics</i>		
R^2	0.9217	0.9902
Q_e (mg/g)	1.2558	1.2586
K_2 (g/mg ⁻¹ min ⁻¹)	0.046	0.1151
<i>Assessment of intraparticle diffusion model</i>		
R^2	0.8749	0.9215

the model and the adsorption system. For the adsorption of RAD on U-TP and T-TP, the equilibrium binding constants, or " K_T " (L/g), were 3.0583 and 1.4914, respectively. The number of functional groups that are available (such COOH and OH) on an adsorbent's surface increases with increasing " K_T " magnitude.

(4) Dubinin-Radushkevich isotherm

The influence of the porous structure of adsorbents was described by Dubinin-Radushkevich's isothermal model. It was predicated on the idea that adsorption was connected to filling the micropore volume rather than layer-by-layer adsorption on the pores' walls and was based on the notion of adsorption potential Eq. (17) providing the Dubinin-Radushkevich isotherm's mathematical expression:

$$Q_e = Q_{DR} e^{-\beta \epsilon^2} \quad (17)$$

The following equation, Eq. (18), represents the D.R model linearly:

$$\ln Q_e = \ln Q_{DR} - K_{DR} \epsilon^2 \quad (18)$$

where Q_{DR} is the theoretical maximum adsorption capacity of D.R model, ϵ is Polanyi's potential as expressed in Eq. (19), and k_{DR} (mol² kJ⁻²) is the isothermal constant of D.R (Hu and Zhang 2019).

$$\epsilon = RT \ln \left(1 + \frac{1}{C_e} \right) \quad (19)$$

where T (K) is the absolute temperature, Q_{DR} (mg/g) is the maximum adsorption capacity in micropores, Q_e (mg/g) is the adsorption capacity at equilibrium, and R is the ideal gas constant (8.314 J/ mol K).

It is possible to compute the average free energy of adsorption (kJ/mol) using Eq. (20) (Al-Wabel et al. 2020).

$$E = \sqrt{\frac{1}{2K_{DR}}} \quad (20)$$

We obtain Q_{DR} and k_{DR} by plotting $\ln(Q_e)$ as a function of ϵ^2 in Fig. 6(D). Neither the physical nor chemical features of the process can be explained by Langmuir's isotherm constants. Nonetheless, the DR isotherm's calculation of average energy of adsorption (E) yields crucial information on these characteristics: The sorption process is dominated by physisorption if E is less than 8 kJ/mol, and by ion exchange (chemisorption) if E is between 8 and 16 kJ/mol. The adsorption energies for untreated and treated peels in this work are 7.91E+03 kJ/mol, 1.00E+04 kJ/mol, respectively, indicating that chemical forces dominate the adsorption process at all temperatures (Bagheban Shahri et al., 2018a).

Adsorption kinetics in batches

Dye adsorption on (U-TP along with T-TP) has been studied using pseudo-first- and pseudo-second-order kinetics.

(1) Study of *pseudo*-first-order kinetics

The general form of Lagergren's equation for this kinetic energy is shown in Eq. (21) (Bagheban Shahri et al. 2018b).

$$\ln(q_{eq}-q_t) = [\ln(q_{eq}) - (k_1 t)] \quad (21)$$

The quantity of RAD taken at equilibrium is represented by " q_e " (mg/g), and adsorption capacity in "mg" of dye at time t (min⁻¹) on 1.4 g and 2.0 g of U-TP and T-TP, respectively, is represented by " q_t " (mg/g) and for pseudo-first-order kinetics, the data obtained from experiments rate constant are indicated by " K_1 ." Adsorptive expulsion of RAD on and simple and tartaric acid-modified biosorbents U-TP and T-TP, respectively, is shown in a plot time "versus" $\ln(q_e - q_t)$ in Fig. 7A.

Table 5 displays the related characteristic parameters. The adsorption of RAD on U-TP and T-TP had correlation values R^2 of 0.53 and 0.71, respectively. The reduced R^2 values for dye on every adjusted adsorbent indicate that according to Lagergren's equation in connection (17), the pseudo-first-order process is not sufficiently applicable to the entire procedure for adsorption.

(2) *Pseudo*-2nd order

HO and McKay provided the rate Eq. (22) for the pseudo-second-order process, which is as follows (Ho et al. 2000):

$$\frac{t}{q_t} = \left[\left(\frac{1}{K_2 q_{eq}^2} \right) + \left(\frac{t}{q_{eq}} \right) \right] \quad (22)$$

The ideal adsorption capacity is indicated by Q_{eq} (mg/g) in the equation above, whereas the adsorption effectiveness with time is shown by. K_2 is the name given to an experimental data rate factor.

The graph showed a linear plot between (q_t vs. t), and the correlational assessment is visually shown in Fig. 7B. Equation (8) computes the rate constants and adsorption capacities

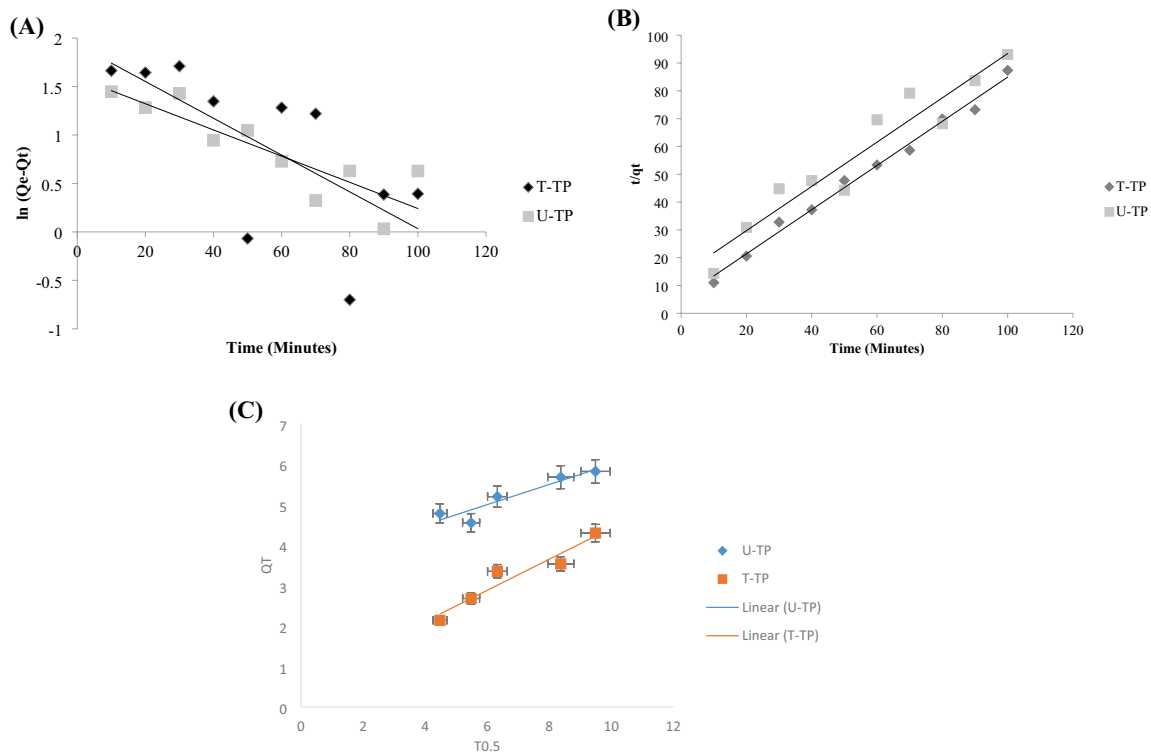


Fig. 7 **A** An analysis comparing the pseudo-first-order kinetics of basic and acid-treated biosorbents' adsorptive dye removal capabilities. **B** A comparison of Rhodamine-B dye removal capabilities in

untreated and tartaric acid treated *Trapa natan* peels using pseudo-second-order kinetics. **(c)**: RAD adsorption on untreated (U-TP) and treated (T-TP) using an intraparticle diffusion kinetic model

from the slope based on these data. Table 5 contains a list of the determined important parameters. Adsorption of dye on U-TP as well as T-TP showed correlation coefficients (R^2) of 0.9217 and 0.9902, respectively, which were close to unity. When results are compared to the pseudo-first-order kinetic model, the pseudo-second-order kinetic model better matches the data.

Intraparticle diffusion model

As its name implies, the kinetic model of intra-particle diffusion created by Weber and Morris is based on the adsorbate's diffusion up until it penetrates the adsorbent. The model's empirical equation found in Eq. (23):

$$Q_t = K_{ID}\sqrt{t} + I \quad (23)$$

where I (mg/g) is the boundary layer thickness, t is the contact duration (min), k_{ID} is the intra-particle diffusion model constant ($\text{mg g}^{-1} \text{min}^{-1/2}$), and Q_t is the adsorption capacity at time t (mg/g) (Weber Jr and Morris 1963). Weber and Morris state that a straight line passing through the origin of the contact information should appear on the graph Q_t vs. \sqrt{t} if intra-particle diffusion is the limiting phase in the adsorbate elimination process. The straight lines in Fig. 7c are not

through the origin, as can be observed. This departure from the origin or close to saturation may be caused by a variation in mass transfer speed between the start and end stages of adsorption. It appears that there were additional mechanisms restricting the onset of the adsorption process besides intraparticle diffusion (Mohanty et al. 2005). Table 5 presents the values of K_{ID} , I , and the coefficient of determination R^2 that were obtained for the plots (Şenol et al. 2024).

(3) Thermodynamic analysis

The study investigated the effects of temperature variations on the optimization of parameters for RAD adsorption. The optimal adsorption percentage ejection of Rad was found to be 65.33% at 50 °C on U-TP and 90.94% at 80 °C on T-TP, indicating that temperature is closely related to adsorption processes. Highest temperatures cause the adsorption process to proceed more slowly because, according to the literature, adsorption is often temperature-dependent (Zhao et al. 2011).

As seen in Fig. 8A, high temperatures increase dye adsorption due to degraded adsorbent structures, causing adsorbents to enlarge, protrude, and lengthen, allowing dye (RAD) to penetrate deeper into the degraded structure. As a result, the rate of adsorption rises. For instance, dye adsorption on U-TP rose from 40 to 50 °C (64 to 65%), but dye adsorption on T-TP kept rising from 70 to 80 °C (87 to 90%).

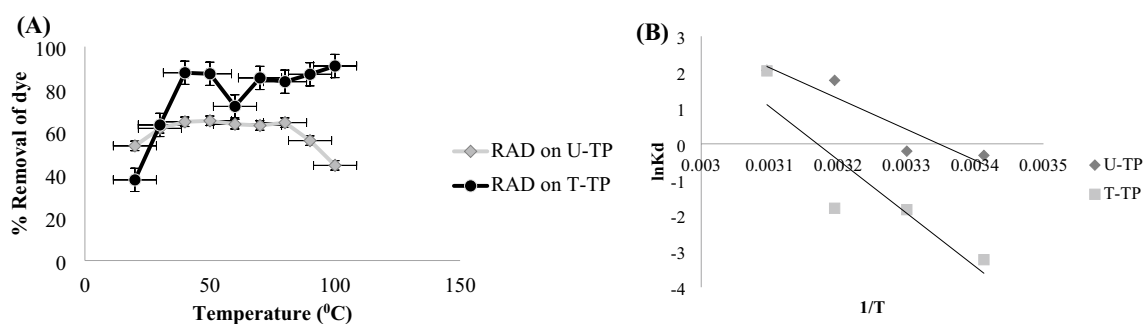


Fig. 8 (A). Effect of change in temperature on removal of Rhodamine-B. (B): A comparison of dye withdrawal capabilities of simple and tartaric acid-treated adsorbent using thermodynamics parameters

Table 6. Thermodynamic evaluation of RAD phytofiltration by simple and tartaric acid-treated peels

Tem (K)	ΔH^0 (kJ/mol)	ΔS^0 (J/mol.K)	ΔG^0 (kJ/mol)
<i>U-TP</i>			
293	71.425574	239.052	-69.971
303			-72.362
313			-3.3978
323			-5.7884
<i>T-TP</i>			
293	123.32156	390.883	-114.41
303			-72.31
313			-122.28
323			-126.13

As a result, in certain circumstances, adsorption increases at significant temperature changes.

Temperature variations impact adsorption and RAD kinetic energy, accelerating dispersion due to the porous interface of cellulosic biomass. Table 6 shows that activation energy, variations in Gibbs free energy, enthalpy, and entropy are examples of basic thermodynamic parameters that regulate the effectiveness and pace of dye adsorption on biosorbent U-TP along with T-TP. An accelerated, endothermic, and spontaneous adsorption process is indicated by the simple and distinct tartaric acid-treated adsorbents. The following equation was used to approximate these calculations:

$$\Delta G^{\circ} = [RT(\ln K_D)] \quad (24)$$

When the temperature in Kelvin is represented by "T," the universal gas constant is represented by "R," and the distribution coefficient, or K_D , is calculated using the formula below.

$$K_D = \frac{(C_o - C_e)}{C_e} \quad (25)$$

The range of enthalpy change values ranging from 80 to 200 kJ mol⁻¹ signifies significant interactions that result in chemisorption. A chemical analysis of each RAD's adsorption on U-TP and T-TP was done, and the results are shown in Table 6. Adsorption is encouraged compared to their untreated forms by the tartaric acid adsorbents' higher enthalpy change values, as shown by formula (26).

$$\ln K_D = \left[\frac{\Delta S^{\circ}}{R} - \frac{\Delta H^{\circ}}{RT} \right] \quad (26)$$

The following formula was used to compute the distortion during adsorption at the solid-liquid border, which may alternatively be obtained from the entropy change: A significant rate of adsorption is favored by its large positive values (Mondal and Kar 2018). Figure 8A demonstrates a representation of a linear graph of "ln K_D versus 1/T."

The adsorptive removal of dye values on U-TP and T-TP, expressed as ΔH° and ΔS° , was ascertained using the slope and intercept. To find ΔH° and ΔS° use Eq. (27).

$$\Delta G^{\circ} = \Delta H^{\circ} - T\Delta S^{\circ} \quad (27)$$

Using the Arrhenius equation, for the adsorptive removal of dye on U-TP and T-TP, the energy of activation (E_a) was identified.

$$\ln k = \left[\ln A - \left(\frac{E_a}{RT} \right) \right] \quad (28)$$

Chemisorption process in this experiment is revealed by the data presented in Table 6

Mechanism of phytofiltration of dye

Chemically modified adsorbents T-TP with chelator (tartaric acid) were shown to interact with RAD by adding different additional moieties across their interfacing regions, such as carbonyls, hydroxyl, and carboxylic acids. As demonstrated by FT-IR, these suggestions were also covered and investigated in sections. Figure 9A, B shows a schematic

and suggested contact processes made by T-TP with dye molecules (RAD). On adsorbent surfaces that have been chemically modified, slight Van der Waals interactions include bonding with hydrogen, surface complexion, chelation, exchange of ions (Pereira et al. 2021), and electrostatic charges cause RAD molecules to link chemically.

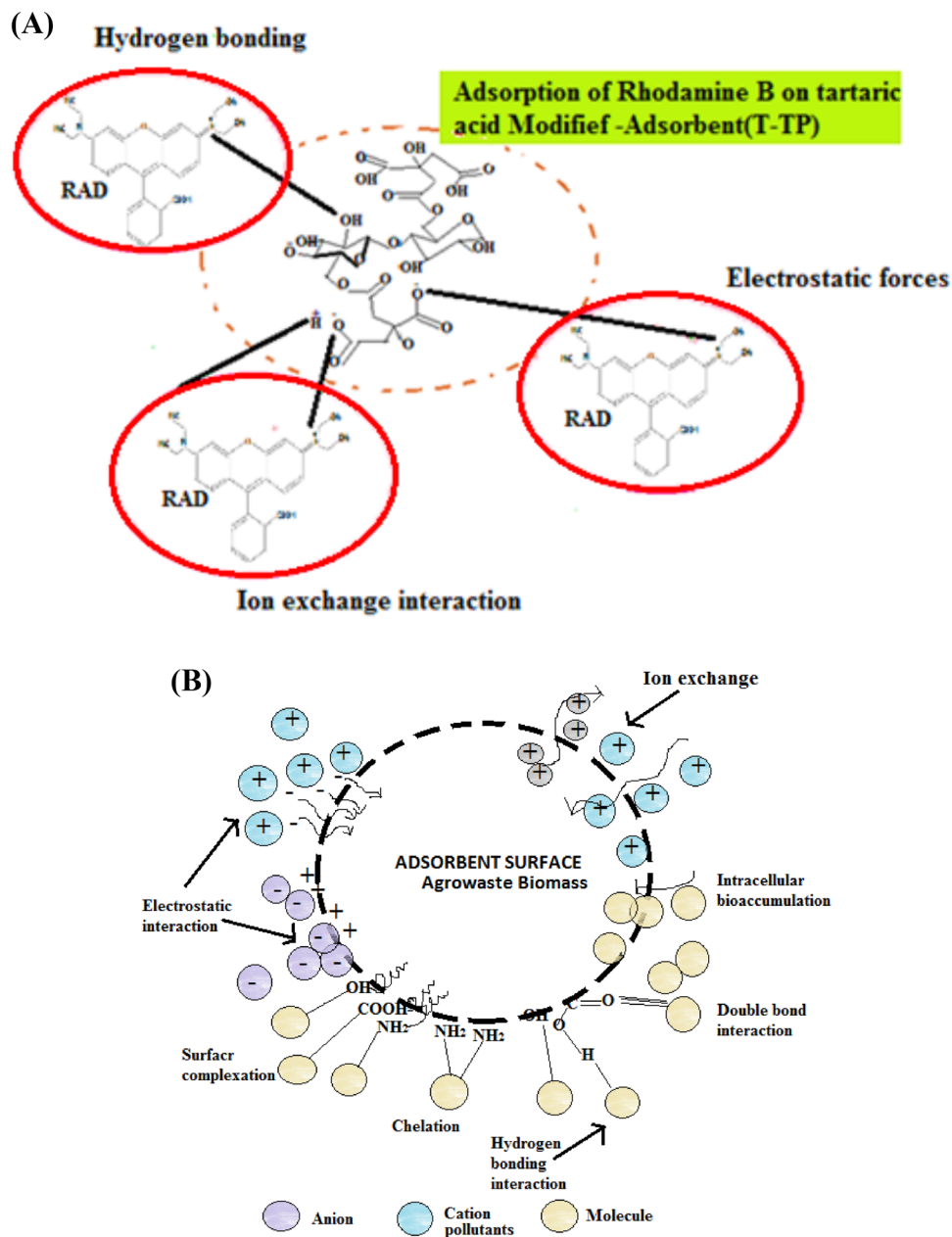
The lignocellulose biomass attraction and adsorption capacity of the newly developed T-TP are described to be enhanced by chemical modification of solid base adsorbents utilizing organic acids such as citric, tartaric, or oxalic. By including additional groups like COOH and OH, this procedure alters and enhances the adsorbents' surface topography, direction, and appearance.

It was observed that the pH of the dye solutions had a significant impact on the adsorption phenomena. This led to the production of negatively charged adsorption sites at the T-TP interface; the ionization of carboxylic acid was closely connected with an increased rate of adsorption. A pH increase was correlated with carboxylic acid deprotonation. As a consequence, the following ion exchange mechanism between H^+ and RAD^+ cations was used:

Desorption process

In order to measure the change in their adsorption effectiveness and to break the adsorbate–adsorbent contacts for

Fig. 9 **A** Diagrammatic representation of the T-TP adsorption process on dye. **B** Adsorbent and dye interactions during proposed phytofiltration of dye molecules



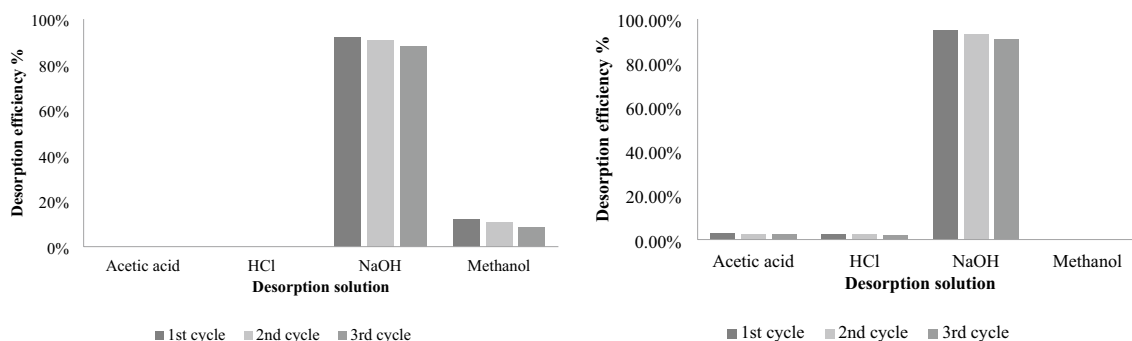


Fig. 10 A Impact of varying desorption solution concentrations on RAD using untreated adsorbent; for desorption efficiency (adsorbent dose = 0.5 g, RAD starting concentration (C_0) = 25 mg L⁻¹). **B**

Impact of varying desorption solution concentrations on RAD dye using tartaric acid treated adsorbent, for desorption efficiency (adsorbent dose = 0.5 g, RAD starting concentration (C_0) = 25 ppm)

future usage, several eluents were used to desorb RAD from the adsorbent. RAD desorption from the used adsorbents has been achieved utilizing the most appropriate desorbing agent, 0.1 M at NaOH (Amran et al. 2021), while the high concentration was ignored because it might damage and deteriorate the crystalline structure and coordination of cellulosic biomasses, which would reduce their ability to adsorb substance. In this experiment, the optimum desorption value of RAD with treated adsorbent was 94.87% and with untreated adsorbent was 91.87%.

With each adsorbent's cycle count increasing, Fig. 10A, B illustrates how the adsorptive performance of the biomass reduced. RAD's desorption was significantly increased with reducing the protons in adsorbents in the pH range of 4–12. This was attributed to repulsion toward the negative binding sites of adsorbents by an ion exchange mechanism.

The following formula was used to determine the adsorbent's desorption capacity and the proportion of RAD that was absorbed (Hussain et al. 2022b):

$$\text{Desorption of dye (\%)} = \frac{q_{\text{desorption}} \left(\frac{\text{mg}}{\text{g}} \right)}{q_{\text{absorption}} \left(\frac{\text{mg}}{\text{g}} \right)} \times 100 \quad (29)$$

Conclusion

The study examined the efficacy of preparing *Trapa natans* peels with tartaric acid to remove harmful and carcinogenic colors from industrial waste water. The presence of extra oxygen-containing groups, such as –COOH and –OH, improved adsorption effectiveness, as shown by FT-IR and SEM analysis as altering the surface modification. The maximum adsorption capacity (Q_{max}) for dye on U-TP measured 2.8801, and on T-TP, the value was 5.5803 mg/g. With strong Langmuir isotherm regression

coefficients suggested a monolayer adsorption process with homogenous chemisorption on active binding sites plentiful on T-TP surfaces. The pseudo-second-order kinetic model, with correlation coefficients (R^2) of 0.92 and 0.99, better fits the data for the adsorption of RAD on U-TP and T-TP. The adsorption mechanism was assessed for endothermic and spontaneous adsorption in both untreated and treated biosorbents as compared to previously published biosorbents, as represented in Table 3. They have significantly improved adsorption capacity with more selectivity for desired pollutant removal. In short, these innovative adsorbent materials are significantly more effective in removing cationic dyes and persistent pollutants using local resources. Taking into account various factors, like: expenses, effectiveness, and ecological consequences, biosorption technique is chosen as a suitable approach for wastewater treatment using minimal resources for removal of dyes from wastewater before discharging it into main water streams.

Acknowledgements The authors thank the Researchers Supporting Project number (RSP2024R169), King Saud University, Riyadh, Saudi Arabia, for the financial support.

Authors contributions Asfa Bajwa helped in initial drafting, laboratory work, Rabia Rehman was involved in supervisor, editing and graphics, Sibgha Ayub performed results graphics and discussion, Muhammad Raza Malik helped in laboratory work and drafting, Sabah Ansar contributed to funding resources and adsorbent characterization, Liviu Mitu helped in characterizational studies, Fadi Alakhras was involved in kinetic studies discussion.

Funding This study was funded by the Researchers Supporting Project number (RSP2024R169), King Saud University, Riyadh, Saudi Arabia.

Data availability statements No datasets were generated or analyzed during the current study.

Declarations

Conflict of Interest The authors declare no competing interests.

References

- Adeleke R, Saidu H, Usman B (2023) Adsorptive removal of Rhodamine B dye from aqueous solution using raw plantain peel. *Afr J Manag Eng Technol* 1
- Affat SS (2021) Classifications, advantages, disadvantages, toxicity effects of natural and synthetic dyes: a review. *Univ Thi-Qar J Sci* 8:130–135
- Al-Wabel MI, Ahmad M, Usman AR, Sallam AS, Hussain Q, Binyameen RB, Shehu MR, Ok YS (2020) Evaluating the efficiency of different natural clay sediments for the removal of chlortetracycline from aqueous solutions. *J Hazard Mater* 384:121500
- Alashkar A, Hassabo AG (2021) Recent use of natural animal dyes in various field. *J Textiles Coloration Polym Sci* 18:191–210
- Amran F, Zaini MAA, INNOVATION (2021) Sodium hydroxide-activated Casuarina empty fruit: Isotherm, kinetics and thermodynamics of methylene blue and congo red adsorption. *Environ Technol* 23:101727
- Anfar Z, Ait Ahsaine H, Zbair M, Amedlous A, Ait El Fakir A, Jada A, El Alem N (2020) Recent trends on numerical investigations of response surface methodology for pollutants adsorption onto activated carbon materials: a review. *J Crit Rev Environ Sci Technol* 50:1043–1084
- Askary M, Behdani MA, Mollaei H, Fallahi HR, Azarmi-Atajan F, Macinaei HM (2024) Bioactive compounds and apoptotic effects of saffron (*Crocus sativus* L.) in different fertilizer conditions. *Biochem Syst Ecol* 114:104806
- Bagheban Shahri F, Niazi A, Akrami A (2018) Application of full factorial design for removal of polycyclic aromatic dye from aqueous solution using 4A zeolite: adsorption isotherms, thermodynamic and kinetic studies. *Polycyclic Aromat Compd* 38:141–156
- Bagheban-Shahri F, Niazi A, Akrami AJ (2018b) Application of full factorial design for removal of polycyclic aromatic dye from aqueous solution using 4A zeolite: adsorption isotherms, thermodynamic and kinetic studies. *38:141–156*
- Banu ZW, Dasgupta D, Hazarika I, Laloo D, Kalita JM (2023) *Trapa natans* L.: a journey from traditional to contemporary therapies—a review. *Nat Prod J* 13:122–134
- Benjelloun M, Miyah Y, Bouslamti R, Nahali L, Mejbar F, Lairini S (2022) The fast-efficient adsorption process of the toxic dye onto shells of walnut and peanut: experiments, equilibrium, thermodynamic, and regeneration studies. *Chem Africa* 5:375–393
- Cabas BM, Icier F (2021) Ohmic heating-assisted extraction of natural color matters from red beetroot. *Food Bioprocess Technol* 14:2062–2077
- Cojocariu B, Mocanu AM, Nacu G, Bulgariu L (2018) Possible utilization of PET waste as adsorbent for Orange G dye removal from aqueous media. *Desalination Water Treatment* 104:338–345
- Coskun R, Savci S, Delibas A (2018) Adsorption properties of activated almond shells for methylene blue (MB). *Environ Res Technol* 1:31–38
- Dutta R, Nagarjuna TV, Mandavgane SA, Ekhe JD (2014) Ultrafast removal of cationic dye using agrowaste-derived mesoporous adsorbent. *Ind Eng Chem Res* 53:18558–18567
- Ferreira JA, Tahezadeh MJ (2020) Improving the economy of lignocellulose-based biorefineries with organosolv pretreatment. *Bioresour Technol* 299:122695
- Geçgel Ü, Özcan G, Gürpınar GÇ (2013) Removal of methylene blue from aqueous solution by activated carbon prepared from pea shells (*Pisum sativum*). *J Chem*
- Ghibate R, Senhaji O, Taouil R (2021) Kinetic and thermodynamic approaches on Rhodamine B adsorption onto pomegranate peel. *Case Studies Chem Environ Eng* 3:100078
- Gören M, Murathan HB, Nihan K, Murathan AM (2021) Removal of Rhodamine B from aqueous solution by using pine cone activated with HNO₃. *J Int Environ Appl Sci* 16:123–132
- Guo X, Liu Z, Tong Z, Jiang N, Chen W (2023) Adsorption of Rhodamine B from an aqueous solution by acrylic-acid-modified walnut shells: characterization, kinetics, and thermodynamics. *Environ Technol* 44:1691–1704
- Gupta VK (2019) Fundamentals of natural dyes and its application on textile substrates. *Chem Technol Natural Synthetic Dyes Pigments*
- Hasanah U, Islam MM (2024) Natural dyes in leather technology. Elsevier, *Renewable Dyes and Pigments*
- Heba O, Ali S, Abdullah N (2019) Chelate coupling with pineapple leaves as a modified bio-sorbent for lead ions (II) removal. *Int J Environ Sci Technol* 16:7293–7304
- Ho YS, Ng J, Mckay GJS, Methods P (2000) Kinetics of pollutant sorption by biosorbents. *29:189–232*
- Hu Q, Zhang Z (2019) Application of Dubinin-Radushkevich isotherm model at the solid/solution interface: a theoretical analysis. *J Mol Liq* 277:646–648
- Hussain MS, Rehman R, Imran M (2021) Isothermal and Kinetic Investigation of Exploring the Potential of Citric Acid-Treated *Trapa natans* and *Citrullus lanatus* Peels for Biosorptive Removal of Brilliant Green Dye from Water. *J Chem* 2021:6051116
- Hussain MS, Rehman R, Imran M (2022a) Comparative evaluation of the adsorption performance of citric acid-treated peels of *trapa natans* and *citrullus lanatus* for cationic dyes degradation from water. *J Chem* 2022:1109376
- Hussain MS, Rehman R, Imran M, Dar A, Akram M, Al-Abbada EA (2022b) Eco-friendly detoxification of congo red dye from water by citric acid activated bioadsorbents consisting of watermelon and water chestnuts peels collected from indigenous resources. *Adsorpt Sci Technol* 2022:9056288
- Imam SS, Babamale HF (2020) A short review on the removal of Rhodamine B dye using agricultural waste-based adsorbents. *Asian J Chem Sci* 7:25–37
- Kabir MM, Akter MM, Khandaker S, Gilroyed BH, Didar-Ul-alam M, Hakim M, Aual MR (2022) Highly effective agro-waste based functional green adsorbents for toxic chromium (VI) ion removal from wastewater. *J Mol Liq* 347:118327
- Khan TA, Nazir M, Khan EA (2013) Adsorptive removal of rhodamine B from textile wastewater using water chestnut (*Trapa natans* L.) peel: adsorption dynamics and kinetic studies. *Toxicol Environ Chem* 95:919–931
- Kolahalam LA, Prasad K, Krishna PM, Supraja N (2024) Lawsonia inermis plant-based cobalt oxide nanoparticles: synthesis, characterization and their biological studies. *Results Chem* 7:101367
- Kumar GP, Pydiraju YB, Lokesh G, Likith USJWCS, ENGINEERING (2023) Removal of Rhodamine B using three adsorbents: isothermal. *Kinetic ANN Model Stud* 8:17
- Kumar S, Patra C, Narayanasamy S, Rajaraman PV (2020) Performance of acid-activated water caltrop (*Trapa natans*) shell in fixed bed column for hexavalent chromium removal from simulated wastewater. *Environ Sci Pollut Res* 27:28042–28052
- Lellis B, Fávoro-Polonio CZ, Pamphile JA, Polonio JC (2019) Effects of textile dyes on health and the environment and bioremediation potential of living organisms. *Biotechnol Res Innovation* 3:275–290
- Mahmud KN, Wen TH, Zakaria ZA (2021) Activated carbon and biochar from pineapple waste biomass for the removal of methylene blue. *Environ Toxicol Manag* 1:30–36
- Mansour RAE-G, Sameda MG, Zaatout AA (2021) Removal of brilliant green dye from synthetic wastewater under batch mode using chemically activated date pit carbon. *RSC Adv* 11:7851–7861
- Mendhekar SY, Rachh PR (2023) Pharmacognostic, physicochemical and preliminary phytochemical investigation of *Trapa natans* linn. root. *Res J Pharm Technol* 16:5444–5452

- Mittal J, Thakur V, Mittal A (2013) Batch removal of hazardous azo dye Bismark Brown R using waste material hen feather. *Ecol Eng* 60:249–253
- Mohanty K, Das D, Biswas M (2005) Adsorption of phenol from aqueous solutions using activated carbons prepared from *Tectona grandis* sawdust by $ZnCl_2$ activation. *Chem Eng J* 115:121–131
- Mohapi M, Sefadi JS, Mochane MJ, Magagula SI, Lebelo K (2020) Effect of LDHs and other clays on polymer composite in adsorptive removal of contaminants: a review. *Crystals* 10:957
- Mondal NK, Kar S (2018) Potentiality of banana peel for removal of Congo red dye from aqueous solution: isotherm, kinetics and thermodynamics studies. *Appl Water Sci* 8:1–12
- Mukhlis MZB, Nazibunnesa S, Islam S, Al-Mahmood AS, Uddin MT (2023) Preparation of chemically and thermally modified water caltrop epicarp (*Trapa natans* L.) adsorbent for enhanced adsorption of Ni (II) from aqueous solution. *Heliyon* 9
- Nascimento RJ, Pereira KRA, Avelino F (2021) Parametric and modeling studies of Rhodamine-B adsorption using coconut coir-based materials as eco-friendly adsorbents. *J Environ Chem Eng* 9:105943
- Nsubuga D, Banadda N, Kabenge I, Wydra KD (2021) Potential of jackfruit waste as anaerobic digestion and slow pyrolysis feedstock. *J Biosyst Eng* 46:163–172
- Ozdemir MB, Karadag R (2023) Madder (*Rubia tinctorum* L.) as an economic factor under sustainability goals in the textile dyeing. *J Natural Fibers* 20:2128968
- Pannacci E, Farneselli M, Monni V, Tei F (2024) Effects of pre-emergence herbicides on weed control and yield of safflower (*Carthamus tinctorius* L.) in Central Italy. *Agronomy* 14:482
- Pereira AG, Rodrigues FH, Paulino AT, Martins AF, Fajardo AR (2021) Recent advances on composite hydrogels designed for the remediation of dye-contaminated water and wastewater: a review. *J Clean Prod* 284:124703
- Rehman R, Anwar J, Mahmud T, Salman M, Shafique U, Zaman W (2011) Removal of murexide (dye) from aqueous media using rice husk as an adsorbent. *J Chem Soc Pak* 33:598
- Rehman R, Hussain MS, Samin G, Jahangir MM, Dar A, Al-Thagafi ZT, Alsantali RI, Al-Abbad EA, Akram M (2024) Effective application of citric acid treated *Trapa natans* and *Citrullus lanatus* lignocellulosic macromolecules for adsorptive remediation of acid Violet-7 dye. *Int J Biol Macromol* 256:128285
- Rehman R, Salariya B, Mitu L (2016) Batch scale adsorptive removal of brilliant green dye using *Trapa natans* peels in cost effective manner. *Revue Chimique* 67:1333–1337
- Savci S (2017) Treatment of biodiesel wastewater using yellow mustard seeds. *Turkish J Eng* 1:11–17
- Savci S, Kemiklioglu E (2017) Removal of Malachite Green a cationic dye from wastewater via adsorption on fish bones. *Fresenius Environ Bull* 26:3078–3084
- Seçme H, Savcı S (2018) Dye removal by adsorption from aqueous solution using pulp (*Nigella sativa*). *Çukurova Üniversitesi Mühendislik-Mimarlık Fakültesi Dergisi* 33:147–154
- Selvakumar A, Rangabhashiyam S (2019) Biosorption of Rhodamine B onto novel biosorbents from *Kappaphycus alvarezii*, *Gracilaria salicornia* and *Gracilaria edulis*. *Environ Pollut* 255:113291
- Senol ZM, Centinkaya S, Arslanoglu H (2023) Recycling of Labada (Rumex) biowaste as a value-added biosorbent for rhodamine B (Rd-B) wastewater treatment: biosorption study with experimental design optimisation. *Biomass Conversion and Biorefinery* 13:2413–2425
- Şenol ZM, Keskin ZS, Dinçer E, Ayed AB (2024) Influential lead uptake using dried and inactivated-fungal biomass obtained from *Panaeolus papilionaceus*: biological activity, equilibrium, and mechanism. *Biomass Conversion and Biorefinery*, 1–12
- Sharma J, Sharma S, Bhatt U, Soni V (2022) Toxic effects of Rhodamine B on antioxidant system and photosynthesis of *Hydrilla verticillata*. *J Hazardous Mater Lett* 3:100069
- Shrestha D (2021) Efficiency of wood-dust of *Dalbergia sisoo* as low-cost adsorbent for Rhodamine-B dye removal. *Nanomaterials* 11:2217
- Singh M, Tiwari D, Bhagat M (2020) Batch adsorption studies on the removal of amaranth red dye from aqueous solution using activated *Trapa natans* peels. *Poll Res* 39
- Soylak M, Unsal YE, Yilmaz E, Tuzen M (2011) Determination of Rhodamine B in soft drink, waste water and lipstick samples after solid phase extraction. *Food Chem Toxicol* 49:1796–1799
- Thakur A, Kaur H (2016) Removal of hazardous Rhodamine B dye by using chemically activated low cost adsorbent: Pine cone charcoal. *Int J Chem Phys Sci* 5:17–28
- Vinod V, Kailash D, Suresh C, Madan L (2012) Adsorption studies of Zn (II) ions from wastewater using *Calotropis procera* as an adsorbent. *Res J Recent Sci* 2277:2502
- Wang Y, Yang X, Jing X, Dai J, Dong M, Yan Y (2020) Adsorption of phosphorus on lanthanum doped carbon films guided by self-assembly of cellulose nanocrystalline. *J Mol Liq* 319:114148
- Wang Z, Gu SJR (2018) State-of-the-art on the development of ultrasonic equipment and key problems of ultrasonic oil production technique for EOR in China. *Renew Sustain Energy Rev* 82:2401–2407
- Weber WJ Jr, Morris JC (1963) Kinetics of adsorption on carbon from solution. *J Sanitary Eng Div* 89:31–59
- Wu J, Yang J, Huang G, Xu C, Lin B (2020) Hydrothermal carbonization synthesis of cassava slag biochar with excellent adsorption performance for Rhodamine B. *J Clean Prod* 251:119717
- Yang G, Li Y, Yang S, Liao J, Cai X, Gao Q, Fang Y, Peng F, Zhang S (2021) Surface oxidized nano-cobalt wrapped by nitrogen-doped carbon nanotubes for efficient purification of organic wastewater. *Sep Purif Technol* 259:118098
- Zango ZU, Imam SS (2018) Evaluation of microcrystalline cellulose from groundnut shell for the removal of crystal violet and methylene blue. *Nanosci Nanotechnol* 8:1–6
- Zhang L, Leung MY, Boriskina S, Tao X (2023) Advancing life cycle sustainability of textiles through technological innovations. *Nature Sustain* 6:243–253
- Zhao X, Zhang G, Jia Q, Zhao C, Zhou W, Li WJCEJ (2011) Adsorption of Cu (II), Pb (II), Co (II), Ni (II), and Cd (II) from aqueous solution by poly (aryl ether ketone) containing pendant carboxyl groups (PEK-L): equilibrium, kinetics, and thermodynamics. *Chem Eng J* 171:152–158
- Zhi LL, Zaini MAA (2019) Rhodamine B dyes adsorption on palm kernel shell based activated carbons. *Malaysian J Fundam Appl Sci* 15:743–747

Publisher's Note Springer Nature remains neutral with regard to jurisdictional claims in published maps and institutional affiliations.

Springer Nature or its licensor (e.g. a society or other partner) holds exclusive rights to this article under a publishing agreement with the author(s) or other rightsholder(s); author self-archiving of the accepted manuscript version of this article is solely governed by the terms of such publishing agreement and applicable law.

Authors and Affiliations

Asfa Bajwa¹ · Rabia Rehman¹ · Sibgha Ayub¹ · Muhammad Raza Malik¹ · Sabah Ansar² · Liviu Mitu² · Fadi Alakhras^{3,4}

✉ Rabia Rehman
rabia.chem@pu.edu.pk; grinorganic@yahoo.com

Asfa Bajwa
asfabajwa18@gmail.com

Sibgha Ayub
sibghaayub108@gmail.com

Muhammad Raza Malik
chemistofpu@gmail.com

Sabah Ansar
sansar@ksu.edu.sa

Liviu Mitu
ktm7ro@yahoo.com; liviu.mitu@upb.ro

Fadi Alakhras
fadialakhras@gmail.com

¹ Centre for Inorganic Chemistry, School of Chemistry, University of the Punjab, Quaid-e-Azam Campus, Lahore 54590, Pakistan

² Department of Clinical Laboratory Sciences, College of Applied Medical Sciences, King Saud University, P.O. Box 10219, Riyadh 11433, Saudi Arabia

³ UNSTPol. Bucharest, Pitesti University Center, 110040 Pitesti, Romania

⁴ Chemistry Department, College of Science, Jerash University, Jerash, Jordan